Journal of Materials Chemistry A

Accepted Manuscript

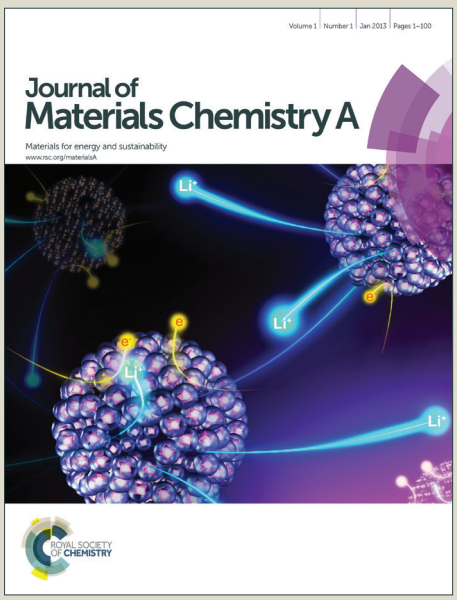

ROYAL SOCIETY OF CHEMISTRY

www.rsc.org/materialsA

Investigating the physical and electrochemical effects of cathodic polarization treatment on TaO_x

Zaenal Awaludin[†], *Mohd Safuan, Takeyoshi Okajima, Takeo Ohsaka*[*]

Department of Electronic Chemistry, Interdisciplinary Graduate School of Science and Engineering, Tokyo Institute of Technology, 4259-G1-5 Nagatsuta, Midori-ku, Yokohama 226-8502, Japan.

Abstract: In the development of non-noble metal electrocatalysts, tantalum oxide (TaO_x)-based materials possess promising potentials due to the high corrosion resistance. In the stoichiometric and bulk form, however, the oxide is extremely inactive. Here, we explored the effects of electrochemical reduction treatment on the physical and electrochemical properties of TaO_x. The oxide is electrochemically deposited on a glassy carbon electrode. The treatment employs a cyclic voltammetry technique in sulfuric acid solution and requires no heat treatment. The X-ray photoelectron spectroscopy (XPS) measurements demonstrated that the stoichiometric Ta_2O_5 is reduced generating the oxides with predominant oxidation state of 4+. Remarkably, the electrochemically reduced TaO_x showed a high activity in hydrogen evolution reaction (HER) and oxygen reduction reaction (ORR). These findings suggest that the electrochemically reductive treatment is an effective way to activate the TaO_x for the electrocatalytic reactions which could be originated from the suboxide species, i.e., Ta^{4+}.

Keywords: Non-noble metal; Electrocatalysis; Tantalum oxide; Electrochemical reduction; XPS

[†]Present address: Department of Research and Development, Permelec Electrode Ltd., 2023-15 Endo, Fujisawa, Kanagawa 252-0816, Japan

[*]Corresponding author: ohsaka@echem.titech.ac.jp

1. Introduction

Recently, tantalum (Ta)-based materials have gained considerably much attention in green technologies. This is because they have been demonstrated as an active catalyst for photocatalysis of water splitting and catalysis of hydrocarbon reactions.[1–3] More importantly, they are also known as electrocatalysts for oxygen reduction reaction (ORR) and hydrogen evolution reaction (HER).[4–12] Along with their robustness in acidic environments, they would be promising alternatives to noble metals which are known to be most active for many electrocatalytic reactions.

Several hypotheses are proposed for origins of the electrocatalytic activities on the Ta-based materials. For example, Ota and co-workers have proposed the importance of oxygen vacancies in tantalum oxynitride ($TaC_xO_yN_z$).[4,12] Meanwhile, Weil et al.[5,13] and Domen et al.[6–8,14] have suggested that particle size is very crucial in determining ORR activity on tantalum oxide (TaO_x) in which the size of less than 4.6 nm gives a high performance. Despite different ideas on the origins of electroactivity, there is a consensus that the suboxide species, e.g., Ta^{4+} possesses a significant contribution in the electrocatalysis.[4–8,10,12–14] In fact, a suboxide species, particularly with low number of electrons filled in its *d* orbital, e.g., d^1, is generally associated with the presence of oxygen vacancy and nonstoichiometric species and often possesses metallic conductivity.[15] The species can also act as active sites in a catalytic reaction.[15–17] One of the examples can be referred to a well-known titanium oxide (TiO_x) in which a Ti^{3+} is regarded as an active site for O_2-adsorption.[16,18] In addition, the presence of suboxide species is also essential for obtaining HER activity on some metal oxides.[19–21]

To produce the active species of Ta, some techniques have been demonstrated to be successful ways. The most common one is a heating treatment which usually requires a high temperature of calcination (up to > 1000 ^oC) under atmospheres of N_2, NH_3 and/or H_2.[4,9,22] Recently, Rossi and co-workers have reported that an electrochemical anodization in

hydrofluoric acid containing solution followed by heating treatment under air atmosphere (800 to 1000 ^{o}C) is successfully applied to produce the active species of Ta^{4+} for catalytic oxidation of CO.[23] An electrochemical technique was also successfully demonstrated by our group in which TaO_x was treated electro-reductively in sulfuric acid solution.[10,24] Although the electro-oxidative treatment via anodic polarization has been routinely used to activate metal oxides, few researchers have utilized the electro-reductive one via cathodic polarization.[19–21,25,26] In fact, to the best of our knowledge, no other researchers have attempted the latter technique to activate TaO_x in aqueous solution.

In the present study, we examined the electrochemical activation of the electrodeposited TaO_x as electrocatalysts for HER and ORR using the electro-reductive treatment via cathodic polarization. We will demonstrate some remarkable results on morphological changes and chemical states which were observed after the electrochemical reduction treatment as well as the high activity in HER and ORR. The effect of electrolyte anions was investigated, revealing that the anions were chemically adsorbed onto the TaO_x affecting its chemical states. Furthermore, the durability of the reduced TaO_x was also studied by exposing it to oxidative and reductive potential regions.

2. Experimental

2.1. Fabrication of TaO_x/GC

The TaO_x/GC electrode was fabricated by simple electrochemical deposition procedure of TaO_x on a glassy carbon (GC) electrode which generally followed that of previous reports.[27,28] All steps in the procedure were carried out at room temperature (set at 25 ^{o}C).

Briefly, a GC electrode (d = 3 mm) was mechanically polished in emery paper No. 600 and 2000, consecutively. Then, it was successively polished using aqueous alumina powder

with size of 1 μm down to 60 nm with the help of polishing microcloth followed by water rinsing with ultrasonication for 10 min. The clean, mirror-like surface electrode was then dried by a commercially available hair drier and was immediately connected into the electrochemical cell containing Ta solution. This solution was prepared by dissolving 0.179 g of $TaCl_5$ (Alfa Aesar) and then 1.064 g of $LiClO_4$ (Wako Pure Chemicals) in 10 mL of propylene carbonate (PC, Kanto Chemicals) solution inside a glove box under Ar gas atmosphere.

Then, the electrodeposition was carried out in a standard three-compartment electrochemical cell. Immediately after the bath solution was prepared, it was poured into the cell, and an Ag wire (d = 1mm) and a graphite plate (4 cm^2) were used as quasi-reference and counter electrodes, respectively. To reduce a possible contamination of water from air atmosphere, the top of the cell was tightly closed by rubber caps. Then, the bath solution was gently bubbled by Ar gas for 15 min to remove possibly dissolved oxygen. Shortly after that, a cyclic voltammetry (CV) was performed by operating ALS/CHI Electrochemical Analyzer (Model 760 Ds) which was controlled by a personal computer. The potential scan was conducted between 0.3 and −2.0 V vs. Ag wire with scan rate of 20 mV s^{-1} for 2 cycles. Just after the deposition, the electrode was immersed respectively in acetone, ethanol and finally water for 1 min each to remove the remaining solution. The as-prepared electrode was then denoted as TaO_x/GC.

The amount of TaO_x deposited on the GC electrode (W_{Ta} in μg cm^{-2}) was calculated using eq 1 below:

$$W_{\mathrm{Ta}}(\mu\mathrm{g\ cm^{-2}}) = \frac{(Q_{\mathrm{dep}} - Q_{\mathrm{blank}})M}{zF} x10^6 \qquad (1)$$

where Q_{dep} and Q_{blank} (in C mol^{-1}) are the total charges of CV response of GC electrode in $LiClO_4$ containing PC solutions in the presence and the absence of $TaCl_5$, respectively, M = 181 g mol^{-1} is the atomic weight of Ta, z = 5 is the number of exchanged electron and F =

96485 C mol^{-1} is the faradaic constant. Thus, this deposition method gave 31.3±0.8 μg_{Ta} cm^{-2} loading of Ta on the GC surface. However, to obtain clear differences of SEM images before and after the electrochemical treatment, which were hardly seen in the previous works [10,24] using this low amount, the TaO_x was deposited by applying five instead of two cycles of the CV deposition. Consequently, the loading amount became 64.4±1.9 $\mu g_{Ta} cm^{-2}$. Although this higher loading caused the lowering in electrocatalytic activities probably due to the lower conductivity, a similar trend of electrochemical behaviors was observed.

2.2. Electrochemical measurements

The electrochemical reduction treatment was also carried out by operating the same ALS/CHI Electrochemical Analyzer as in the Ta electrodeposition. To enhance conductivity of electrolyte that is believed to be more effective for the electrochemical treatment, a 2.0 M H_2SO_4 solution was used as electrolyte. The solution was prepared by diluting the concentrated stock one (Wako pure chemicals).

Briefly, the as-prepared TaO_x/GC electrode was transferred into another three-compartment electrochemical cell in which an $Ag|AgCl|KCl_{(sat)}$ and a GC plate (4 cm^2) were served as reference and counter electrodes, respectively. All the potentials quoted here, except noted, were converted to a reversible hydrogen electrode (RHE). A CV technique was then used for the electrochemical reduction treatment in which the potential range was repeated between 0.0 and −0.7 V with scan rate of 20 mV s^{-1} for 30 up to 1000 cycles. After the electrochemical treatment, the treated TaO_x/GC electrode was taken out from the cell and subjected for various characterizations. For a control experiment, the same procedure was also applied for the bare GC electrode.

2.3. Surface characterizations

Various measurements were performed to characterize the surface properties of electrode. To take the surface pictures for observing a color change, we used a commercially available digital camera and an optical microscope of VN-8010M (KEYENCE) with magnification of ×1250. The images of surface morphology were collected using a field emission scanning electron microscope of S4700 (HITACHI). Meanwhile, the fine details of image were acquired from transmission electron microscopy (TEM) measurements by operating a transmission electron microscope of JEM-2010F (JEOL) with accelerated voltage of 200 kV. For the case of TEM samples, carbon-coated molybdenum grids (d = 3mm) were used as the substrate because the pure carbon one was deformed in a PC solvent.

To examine chemical species on the electrode surface, X-ray photoelectron spectroscopy (XPS) measurements were carried out by operating an ESCA 3400 electron spectrometer (SHIMADZU). For these purposes, the analyzed area of electrode sample was 0.283 cm^2. The measurements were conducted by using unmonochromatized X-ray source (Mg Kα ($h\upsilon$= 1253.6 eV) anode, emission current: 20 mA and acceleration voltage: 10 kV) under an ultra-high vacuum (1 x 10^{-6} Pa) condition. An argon ion (Ar^+) bombardment was performed to investigate the depth profile of TaO_x by which 1.5 keV Ar^+ ions generated from 5x10^{-4} Pa Ar atmosphere were sputtered onto the electrode surface. This etching rate is calculated to be equivalent to 4 Å min^{-1}.[29] To compensate the electrostatic charging, which is usually generated during XPS measurements, the obtained spectra were manually corrected to an internal reference spectra of C 1s at binding energy of 284.5 eV. Then, the corrected spectra were carefully deconvoluted using XPSPEAK 4.1 software. Particularly for the peaks of Ta species, a ratio of the area of Ta $4f_{5/2}$ and Ta $4f_{7/2}$ was fixed to be 1.23 with their binding energy gap of 1.87 eV. Meanwhile, a full width at half maximum value (FWHM) of the peaks was set at binding energy width of 1.4±0.5 eV. These parameters were acquired from the peaks of Ta_2O_5 species which were collected from three samples of the as-prepared

TaO_x/GC electrode.

3. Results and discussion

3.1. Optical surface images

We observed the color change of the surface before and after the electrochemical reduction treatment of the TaO_x/GC electrode (Fig. 1). The as-prepared TaO_x/GC electrode showed as a shiny black surface similarly to the bare GC disk electrode. After the treatment of 1000 cycles, the color of the surface became dark blue which could be seen only under light exposure and at dry condition (Fig. 1a). The change of surface color has been also known for the case of WO_x in which it turns from transparent in the oxidized state to deep blue in the reduced one.[30,31]

To obtain the enlarged, colorful images of the surface, we then performed optical microscopy measurements as shown in Figs. 1b, c and d. For this purpose, we used a GC plate electrode instead of the disk one to fit the sample holder.

Before the TaO_x deposition (Fig. 1b), the GC plate appeared as an inhomogeneous surface where some pores, which were seen as dark areas, still remained even after polishing with the same procedure for the bare GC disk electrode. After the deposition of TaO_x, no apparent changes in the surface color and morphology were observed (Fig. 1c) due to the very low amount of the TaO_x deposits and low magnification. Meanwhile, after the electrochemical treatment (Fig. 1d) the electrode surface became colored with alternate arrangement of blue and green. From these observations, we believe that the color change could be associated with a so-called structural color reflecting the change of TaO_x morphology as we will discuss them in the next sections.[32]

3.2. SEM and TEM characterizations

Electrochemical treatment commonly causes morphological changes of electrode surface. In particular, applying oxidative current produces a surface roughening [23,33,34]. But, sometimes, the reverse effect (i.e., smoothing effect) is observed when the reductive current is applied. For example, Co-oxide film appears as fine particles with size of about 10 nm after exposing them to reductive treatment while anodic one results in the formation of cracks.[35] The change of morphology can also be seen in the present case as demonstrated in the SEM and TEM images (Figs. 2 and 3).

Before the treatment, (Figs. 2a and c), the TaO_x species were seen as irregularly shaped particles with a wide range of size between 10 nm and 1 μm, and they were interconnected to form a framework with the estimated thickness as high as 1 μm. After applying the electro-reductive treatment (Figs. 2b and d), the surface morphology of the TaO_x species was dramatically changed, i.e., the surface structure of the individual particles could not be distinguished. It seemed to become a very fine structure forming a smooth, homogenously compact layer with the thickness of ~25 nm which was thinner than that of the as-prepared TaO_x.

The internal morphology of the deposits was then examined using TEM images (Figs. 3a-f). Before the electrochemical treatment (Figs. 3a and c), the TaO_x deposits were seen to be agglomerated and consequently, to form a thick layered structure, being consistent with the SEM images (Fig. 2a). After the electrochemical treatment (Figs. 3b and d), they apparently become a thinner layer as indicated from its transparency, and some particles of TaO_x with size between 100 and 200 nm were also observed. The TaO_x particles might be integrated to form a thinner layer during the electrochemical treatment, while some of the TaO_x species might still remain as particles.

In the high-resolution images (Figs. 3e and f), a focus was taken on one TaO_x particle for observing its detailed structure. Before the treatment (Fig. 3e), the TaO_x particle was seen to

be amorphous indicated by no apparent lattice fringe, which is consistent with the previous work.[27] After the electrochemical reduction treatment (Fig. 3f), the TaO_x particle seemed to become thinner with some black-dotted spots. According to the EDX data (Fig. 3g) there are some sulfur-containing species adsorbed onto the TaO_x.

3.3. XPS analyses

Another effect that can be expected by the electrochemical reduction of TaO_x/GC electrode is the change of chemical species. The most probable change that is possibly observed is the lowering of oxidation state of Ta from +5 of Ta_2O_5. The other possibility would be the presence of some new elements which may be introduced during the reduction processes of the electrodeposition of Ta and the electro-reductive treatment. To make these possibilities clear, we utilized XPS analyses as summarized in Figs. 4 and 5.

At first, a survey scan was performed in the range of binding energy of 0 to 1000 eV as shown in Fig. 4a. For the sake of clarity, we show only up to 600 eV where the peaks of all possible metal contaminants, e.g., noble metals, can be observed.[20,27] Noticeably, there appeared no peaks of such contaminants but two interesting observations were obtained; (1) the appearance of a new peak at binding energy of 170 eV assigned as S containing species and (2) an enhanced intensity of O response. The former confirms the EDX measurement (Fig. 3g) and is in a good agreement with the previous report for the case of $TaC_xO_yN_z$ during ORR electrocatalysis in sulfuric acid solution.[36]

To address the presence of S containing species further, we examined the S species by focusing the measurement on S 2p spectra as shown in Fig. 4b. Before the CV treatment, no peaks corresponding to S containing species were expectedly observed at the TaO_x/GC electrode. After 30 cycles of the CV treatment, two peaks at binding energies of 169.1 and 160.4 eV assigned as SO_4^{2-} and S/S_2^{2-}, respectively, appeared.[37] However, no further changes

in both intensity and position were observed after 1000 cycles. These results imply that the sulfate anions were chemisorbed on the TaO_x during the electro-reductive treatment followed by its electro-reduction process producing the S/S_2^{2-} species.

Meanwhile, when the same electrochemical treatment was performed for the bare GC electrode (Fig. S1), no significantly intense peaks of S containing species were seen. This concludes that the sulfate anions would be adsorbed not on the GC but specifically on the TaO_x.

In consequence of the adsorption of sulfate, we can suggest that it is strongly related to the enhanced O intensity. Rationally, the four oxygen bonds in the adsorbed sulfate could cause addition of oxygen-containing species on the surface. Thus, this can be reflected in the enhanced intensity of O spectrum as illustrated in Fig. 4c. For example, after 30 cycles of the CV treatment, the intensity of this spectrum increased by about 2.5 times with a shift of binding energy towards higher value by about 1.7 eV. Further increase of the CV treatment up to 1000 cycles unchanged its intensity, but only a slight shift of its binding energy towards lower value was observed. This shift could be ascribed to the change of oxidation state of Ta as discussed later.

Meanwhile, the C 1s spectrum (Fig. 4d), which is used as an internal reference, showed no significant differences before and after the reduction treatment. Only a little decrease of its intensity (10%) in respect to the initial value was measured at the electrode after 1000 cycles of the CV treatment. This might be caused by the formation of a compact layer of TaO_x that hinders the penetration of electron beam into the base.[38]

For the case of Ta_2O_5, it was expected to be reduced by applying the reductive CV treatment generating its reduced species, e.g, Ta^{4+} as in the case of heating treatment.[23] For the sake of clearer observation of XPS spectra, we chose Ta 4f spectrum instead of Ta 5d one because the former possesses more intense response. We summarized the results in Fig. 5a

and Table 1.

In the as-prepared TaO_x/GC electrode, a couple of peaks located at binding energies of 28.7±0.1 and 26.8±0.1 eV were observed (bottom). These peaks are attributed to the responses of Ta $4f_{5/2}$ and Ta $4f_{7/2}$, respectively, belonging to the most stable Ta_2O_5 species. These values are in a good agreement with those early reported by Mathieu and Landolt[39] (28.6±0.2 and 26.8±0.2 eV) and are close to those reported by Ota et al.[36] (28.3 and 26.5 eV). On the other hand, Diaz et al.[40] have reported the relatively lower ones, i.e., 27.9 and 26.0 eV. These slight differences may be due to the differences in preparation methods, deposition substrates and/or the internal references used in XPS measurements.

After 30 cycles of the CV treatment (mid), the Ta_2O_5 peaks unexpectedly shifted towards higher binding energies by 0.4 eV. This shift was also followed by the appearance of a significant portion (25.4%) of reduced TaO_x species at binding energies at 28.3 and 26.4 eV which can be assigned as Ta^{4+}. A further reduction treatment by increasing the number of cycles, i.e., 1000 cycles (top), increased the peak intensity corresponding to the Ta^{4+} which became a dominant species (74.6%). At this stage, the other reduced species located at binding energies of 26.1 and 24.2 eV was also observed and assigned as Ta^{3+} species.

However, a longer time reduction up to 6000 cycles demonstrated that the Ta^{4+} was still the dominant species, i.e., ~75%, without significant increase of the Ta^{3+} fraction.[10] This finding implies that the present reduction technique was able to reduce the Ta^{5+} to produce Ta^{4+} species and less amount of Ta^{3+} species but no species with oxidation states lower than 3+.

One issue of the above results was the positive shift of binding energy by 0.4 eV. This might be caused by the adsorbed sulfate on the TaO_x which is also reported by Ota et al.[36] They monitored a high-energy shift of the Ta_2O_5 by 0.3 eV during ORR which is ascribed to

the formation of Ta-SO_4. The same phenomenon was also reported for other metal oxides due to their intrinsic properties.[41–43]

However, in the present case the sulfate layer seemed to almost completely cover the TaO_x surface. This was strongly indicated from the absence of Ta^{5+} species with binding energies similar to those in the as-prepared TaO_x/GC electrode. To probe this issue, we attempted to etch the sulfate species using Ar^+ bombardment for 1 min (Fig. 5b). As a result, all peaks of the reduced TaO_x moved towards the lower values, and consequently, their binding energies became similar to those of the as-prepared TaO_x/GC electrode. For example, after the Ar^+ etching the peaks of Ta_2O_5 were 28.7 and 26.8 eV which moved negatively from 30.1 and 27.2 eV (before the Ar^+ etching).

Meanwhile, the binding energies of Ta^{4+} became 25.7 and 23.8 eV. These values are by 0.6 eV higher than those reported by Rossi et al..[23] This large difference might be caused by the fact that our values for the Ta_2O_5 are by 0.4 eV higher than their ones. On the other hand, Ota et al. have assigned the Ta 4f peaks with binding energies of 25.9 and 27.9 eV or 0.4 eV lower than those of Ta_2O_5 as the Ta species near to oxygen vacancy defects.[36] Thus, our finding on the formation of Ta suboxide species is consistent with those of previous works in which heat treatments are utilized.

Furthermore, the Ar^+ bombardment could also successfully uncover the real intensity of Ta 4f spectra of the reduced TaO_x/GC electrode which was measured as high as 2.4 times relative to that of the TaO_x/GC electrode before Ar^+ bombardment. More importantly, the etching treatment caused no significant change in the composition of Ta. This can be noticed at the TaO_x/GC after 30 cycles of CV treatment (mid) in which the Ta^{4+} fraction was 25.6% comparable to that before Ar^+ etching (25.4%).

In contrast, the Ar^+ bombardment onto the as-prepared TaO_x/GC electrode (bottom) obviously caused severe surface erosion on the TaO_x resulting in 74% loss of its intensity.

This also resulted in uncovering the composition of the core layer which consists of the oxides with oxidation states of Ta^{4+}, Ta^{3+} and Ta^{2+}. The erosion of layer also occurred on the adsorbed sulfate which was lost by approximately 82% (Fig. S2). Thus, this large destruction of sulfate layer might easily allow the electron penetration during XPS measurement uncovering the real responses of under-layered TaO_x.

3.4. Electrochemical characterizations

Some metal oxides, e.g., WO_3, IrO_2, RuO_2, have been shown as active electrocatalysts for HER.[19–21,44–46] Interestingly, pretreatment of electrode by applying cathodic polarization is necessary to attain the highest HER activity as demonstrated in the very early report by Blouin and Guay.[20] They mentioned that after cathodic polarization for up to 10 h, the HER activity on IrO_2 and RuO_2 increases by as high as 100 times compared with that before the activation.

Similarly, the present treated TaO_x electrode also exhibited a HER activity, i.e., it was significantly increased as the cycle number of reductive CV was increased as shown in Fig. 6a. This figure was constructed by recording the potentials at which a cathodic current reached 1 mA cm^{-2}. Apparently, the potential shifted to the lower value from −0.59±0.10 V at the first cycle to −0.39±0.04 V and −0.19±0.05 V after the 30^{th} and 1000^{th} cycles, respectively.

On the other hand, in the case of bare GC electrode (Fig. S3), although the increased cathodic currents with increasing the cycle number of reductive CV were also observed presumably due to the reduction of graphitic oxides, their intensities were too low compared with those at the TaO_x/GC. This is very reasonable because a bare GC electrode is not active electrocatalyst for HER.

For comparison with previous works, the HER activity was further evaluated by using

linear sweep voltammetry (LSV) at a low scan rate of 5 mV s^{-1} in 0.5 M H_2SO_4 (Fig. 6b). The overpotentials to reach 0.1 mA cm^{-2} were 0.25±0.04 and 0.15±0.04 V for the TaO_x/GC electrode at 30 and 1000 cycles of the CV treatment, respectively. Clearly, the treated TaO_x/GC is significantly superior in HER activity to the $Ta_xC_yN_z$ (~0.25 V).[9] In comparison with other metal oxides, the activity of the treated TaO_x also exceeds that of the WO_x synthesized by hydrothermal method, which requires over 0.40 V of overpotential to reach the same cathodic current [44], but is inferior to that of the WO_x activity prepared by a microwave-assisted hydrothermal method, which is comparable to that of Pt.[46] The reduced TaO_x is also a little inferior to the conductive oxides of noble metals, such as RuO_2 and IrO_2.[19–21]

Some metal oxides, e.g., WO_3, RuO_2 and IrO_2, are also shown to be active not only for reducing proton in acidic solution but also for water reduction in alkaline solution.[19,45–48] Accordingly, we also tested the HER activity of the reduced TaO_x/GC in 0.1 M KOH solution. As can be concluded from the inset of Fig. 6b, no HER activity was noticed at the same potential range as in the acidic solution. This indicates that the reduced TaO_x was unlikely able to reduce water in alkaline solution.

Beside HER activity, TaO_x is also known as an active electrocatalyst for ORR which can be found in refs. 4−8,24. From the references, we summarize that the onset potentials can be observed at potential range between 0.80 and 1.00 V depending on the preparation method. To obtain a steady voltammogram, before the examination of ORR, the electrodes were potentially scanned between 0.05 and 1.30 V at scan rate of 50 mV s^{-1} for 10 cycles in O_2-saturated 0.1 M H_2SO_4 solution. The onset potentials of ORR on the reduced TaO_x/GC and the bare GC electrodes were then measured as summarized in Fig. 7.

We found that the onset potential of the reduced TaO_x was 0.81±0.07 V and much more positive (by 0.74 V) than that of the bare GC electrode treated by the same method. This

value is close to that of the references[4–8] and consistent with our previous result in which the TaO_x was electrochemically reduced using a constant-potential polarization.[24] Here it is noticed that the limiting current at the reduced TaO_x was insignificantly increased compared to that at the bare GC electrode, implying an incomplete 4-electron reduction process at this TaO_x which was confirmed by rotating ring-disk electrode voltammetric measurements.[24]

We should mention here that the ORR activity of the reduced TaO_x/GC electrode was obtained only on the electrode which was treated, as mentioned above, for at least 1000 cycles. For the case of TaO_x/GC electrode treated by 30 cycles, it did not show ORR activity at the potential region between 0.80 and 1.00 V but was still similar to that of the bare GC electrode. It seemed that the electrode suffered from oxidation at potential above 1.0 V during the potential scanning conducted before the measurements of ORR. This might be caused by the unstably small fraction (~25%) of the suboxide species generated by only 30 cycles of the electrochemical treatment (Fig. 5).

Next, the stability of the reduced TaO_x was investigated by potential cycling. It is important to study its feasibility for practical application where electrocatalysts particularly for ORR would be exposed up to potential of 1.5 V.[49] In the previous report, a considerably good stability of TaO_x has been achieved after 1000 cycles of CV test at potentials between 0.6 and 1.23 V.[6]

To create a severer condition that could greatly accelerate the dissolution and detachment of the deposits, the potential region of potential cycling test was extended −0.20 ~ 1.23 V. The negative potential of −0.20 V was set to easily monitor the HER activity without stopping the experiment (Fig. 8). For this purpose, the reduced TaO_x, which was produced by 1000 cycles of the CV treatment, was used as the sample.

At the initial stage, the HER activity became clear after the first 50 cycles in a good agreement with the previous report for the case of ORR.[6] Then, it gradually decreased as

seen from the fact that the cathodic currents decreased from 14.3 to 9.3 mA cm^{-2} (after 350 cycles). We found that the decreased current was caused by some bubbles attached on the electrode surface. Thus, we rigorously removed them without stopping the experiment and as expected, the current was again increased to reach even higher current intensity of 17.1 mA cm^{-2}.

Starting from the stage, although we often removed the bubbles when they were formed and seemed to block the surface, the current was still continuously decreased. Finally, it reached 8.6 mA cm^{-2} or 33% loss in respect to the steady initial current, i.e., after the first 10 cycles. The potential cycling might bring about the oxidation of the reduced TaO_x into the stoichiometric phase, i.e., Ta_2O_5 and presumably, detachment of the deposits. However, the reduced TaO_x could be still considered as a stable electrocatalyst since it its durability surpassed that of other non-noble metal HER electrocatalysts.[37,50] Thus, we believe that the reduced TaO_x would be applicable at least for hydrogen production since this severe condition would barely occur in the real situation.

An intriguing phenomenon observed during the durability test is a dramatic enhancement of HER at the first 10 cycles as shown in the inset of Fig. 8. This was reproducible for all cases of the TaO_x/GC which was treated by at least 1000 cycles and was consistent with what we found for the TaO_x reduced at a constant potential (0.6 V) for 10 h.[24] A similar observation has been also reported on RuO_2 and even on pure Ti electrodes during cathodic and anodic scans, which is suggested to be due to H-chemisorption.[20,45] The oxidation treatment also desorbed the adsorbed sulfate and sulfide layers that might result in generating more active sites of the reduced TaO_x (Fig. S4).

3.5. Origins of the electrocatalysis

Three significant effects of the electrochemical reduction treatment that may contribute

to the electrocatalytic activities were observed in the present results. Firstly, as expected, the XPS data show strong evidences for the formation of Ta^{4+} species. We thus believe that this species may play an important role in the ORR and HER acting as the active sites. This is because a suboxide species possesses a lower work function than in the fully stoichiometric one.[15–17] Thus, the lowering effect may facilitate the adsorption of O_2 and H^+ on the TaO_x, and along with its capability of electron and proton transfers, the electrocatalytic reactions could be enhanced.[51,52]

Secondly, the morphological change of deposits, which was transformed from irregularly shaped deposits to a homogenous layer, might result in increasing the number of active sites. This is supported from the fact that the intensity of Ta 4f spectra increased by 2.4 times (Fig. 5) after the electro-reductive treatment. Furthermore, the thinner thickness produced after the treatment could also further reduce the electrical resistance of the oxide.[53,54]

Thirdly, we also observed the formation of sulfide compounds adsorbed on the TaO_x. Some metal sulfides are known as active HER electrocatalysts in acidic solution [37,55–57]. However, the activity of the metal sulfides is lost by oxidation at potential higher than 0.6 V due to the oxidation of the sulfides resulting in their dissolution into electrolyte as sulfate.[37] This is in contrast to what we found for the reduced TaO_x in which the HER activity was not greatly lost even by oxidation at potential of 1.23 V, albeit the adsorbed sulfides and sulfate were almost completely removed from the TaO_x surface (Fig. S4). Thus, it seems that the sulfide formation on the reduced TaO_x would not participate in the HER activity.

There is also a concern of contribution from unknown impurities that might be introduced during the electrodeposition and reduction treatment. However, as discussed above, based on the XPS measurements, the control experiment of bare GC electrode and the examination of HER activity in alkaline solution we could strongly evidence that no impurities, particularly noble metals participated in the electrocatalysis.

4. Conclusions

The effects of electrochemical reduction treatment on the composition and electrochemical properties of TaO_x were examined. The morphology of the TaO_x apparently changed, i.e., the irregularly shaped deposits became a layer. The Ta_2O_5 layer on the TaO_x/GC electrode was obviously reduced to form its reduced species mainly as TaO_2 with ratio of as high as ~75% with a small fraction of the oxide with oxidation state of 3+. The anions in electrolyte, namely as sulfate, were adsorbed on the TaO_x during the treatment affecting its chemical states in which it became more oxidized state. In the XPS measurements, the chemisorbed sulfate also caused lowering of the intensity of Ta 4f spectra. Thus, an Ar^+ bombardment for 1 min was likely necessary to obtain the real responses. The treated TaO_x showed high electrocatalytic activities for ORR and HER with considerably good durability. These findings suggest that electrochemical reduction technique is an effective way to uncover the hidden potential of TaO_x which was thought to be inactive in their bulk, stoichiometric form.

Acknowledgments

The present work was financially supported by Grant-in-Aid for Scientific Research (A) (No.19206079) to T. O. from the Ministry of Education, Culture, Sports, Science, and Technology (MEXT), Japan and to Z. A. from Tokyo Institute of Technology Global COE Program for Energy Science. Z. A. gratefully acknowledges the Government of Japan for MEXT Scholarship. Authors thank Dr. J. Koki and Dr. D. Lu of the Centre for Advanced Material Analysis at Tokyo Tech for their help in SEM and TEM measurements.

References

1. K. Maeda, K. Domen, *J. Phys. Chem. Lett.*, 2010, **1**, 2655-2661.
2. T. Ushikubo, *Cat. Today*, 2000, **57**, 331-338.
3. Y. Chen, J. L. Fierro, T. Tanaka, I. E. Wachs, *J. Phys. Chem. B*, 2003, **107**, 5243-5250.
4. A. Ishihara, M. Tamura, K. Matsuzawa, S. Mitsushima, K. I. Ota, *Electrochim. Acta*, 2010, **55**, 7581–7589.
5. J. Y. Kim, T. K. Oh, Y. Shin, J. Bonnett, K. S. Weil, *Int. J. Hydrogen Energy*, 2011, **36**, 4557–4564.
6. J. Seo, L. Zhao, D. Cha, K. Takanabe, M. Katayama, J. Kubota, K. Domen, *J. Phys. Chem. C*, 2013, **117**, 11635–11646.
7. J. Seo, D. Cha, K. Takanabe, J. Kubota, K. Domen, *ACS Catal.*, 2013, **3**, 2181-2189.
8. J. Seo, D. H. Anjum, K. Takanabe, J. Kubota, K. Domen, *Electrochim. Acta*, 2014, **149**, 76-85.
9. N. S. Alhajri, H. Yoshida, D. H. Anjum A. T. Garcia-Esparza, J. Kubota, K. Domen, K. Takanabe, *J. Mater. Chem. A*, 2013, **1**, 12606–12616.
10. Z. Awaludin, T. Okajima, T. Ohsaka, *Chem. Lett.*, 2014, **43**, 1248–1250.
11. S. Wirth, F. Harnisch, M. Weinmann, U. Schröder, *Appl. Catal. B*, 2012, **126**, 225-230.
12. T. Asada, M. Arao, K. Kubobuchi, M. Mogi, Y. Takahashi, M. Matsumoto, A. Ishihara, K. I. Ota, H. Imai, *Fuel Cells*, 2014, **14**, 769–774.
13. T. Oh, J. Y. Kim, Y. Shin, M. Engelhard, K. S. Weil, *J. Power Sources*, 2011, **196**, 6099–6103.
14. J. Seo, D. Cha, K. Takanabe, J. Kubota, K. Domen, *Phys. Chem. Chem. Phys.*, 2014, **16**, 895–898.
15. M. T. Greiner, M. G. Helander, W. M. Tang, Z. B. Wang, J. Qiu, Z. H. Lu, *Nat. Mater.* 2012, **11**, 76–81.
16. G. Pacchioni, *Chem. Phys. Chem*., 2003, **10**, 1041-1047.
17. U. Diebold, *Surf. Sci. Rep.*, 2003, **48**, 53–229.
18. C. Di Valentin, G. Pacchioni, A. Selloni, *J. Phys. Chem. C*, 2009, **113**, 20543–20552.
19. J. C. F. Boodts, S. Trasatti, *J. App. Electrochem.*, 1989, **19**, 255–262.

20. M. Blouin, D. Guay, *J. Electrochem. Soc.*, 1997, **144**, 573–581.

21. T. E. Lister, Y. V. Tolmachev, Y. Chu, W. G. Cullen; H. You, R. Yonco, Z. Nagy, *J. Electroanal. Chem.*, 2003, **554**, 71–76.

22. Y. Ohgi, A. Ishihara, K. Matsuzawa, S. Mitsushima, K. I. Ota, M. Matsumoto, H. Imai, *Electrochim. Acta*, 2012, **68**, 192–197.

23. R. V. Gonçalves, R. Wojcieszak, P. M. Uberman, S. R. Teixeira, L. M. Rossi, *Phys. Chem. Chem. Phys.*, 2014, **16**, 5755–5762.

24. Z. Awaludin, T. Okajima, T. Ohsaka, *J. Power Sources*, 2014, **268**, 728–732.

25. M. Senthilkumar, J. Mathiyarasu, J. Joseph, K. L. N. Phani, V. Yegnaraman, *Mater. Chem. Phys.*, 2008, **108**, 403–407.

26. K. Videm, S. Lamolle, M. Monjo, J. E. Ellingsen, S. P. Lyngstadaas, H. J. Haugen, *App. Surf. Sci.*, 2008, **255**, 3011–3015.

27. Z. Awaludin, J. G. S. Moo, T. Okajima, T. Ohsaka, *J. Mater. Chem. A*, 2013, **1**, 14754–14765.

28. Z. Awaludin, M. Suzuki, J. Masud, T. Okajima, T. Ohsaka, *J. Phys. Chem. C*, 2011, **115**, 25557–25567.

29. J. G. S. Moo, Z. Awaludin, T. Okajima, T. Ohsaka, *J. Solid State Electrochem.*, 2013, **17**, 3115–3123.

30. C. Bechinger, M. S. Burdis, J.-G. Zhang, *Solid State Commun*. 1997, **101**, 753–756.

31. D. S. Dalavi, R. S. Devan, R. A. Patil, R. S. Patil, Y. R. Ma, S. B. Sadale, I.-Y. Kim, J.-H. Kim, P. S. Patil, *J. Mater. Chem. C*, 2013, **1**, 3722-3728.

32. S. Cui-Cui, C. Yun-Yu, D. En-Mei, L. Chang-Hao, *Chin. Phys. B*, 2012, **21**, 088101-1–088101-2.

33. N. K. Allam, X. J. Feng, C. A. Grimes, *Chem. Mater.*, 2008, **20**, 6477–6481.

34. H. E. Prakasam, K. Shankar, M. Paulose, O. K. Varghese, C. A. Grimes, *J. Phys. Chem. C*, 2007, **111**, 7235–7241.

35. S. Cobo, J. Heidkamp, P. A. Jacques, J. Fize, V. Fourmond, L. Guetaz, B. Jousselme, V. Ivanova, H. Dau, S. Palacin, M. Fontecave, V. Artero, *Nat. Mater.*, 2012, **11**, 802–807.
36. M. Matsumoto, T. Miyazaki, S. Fujieda, A. Ishihara, K. I. Ota, H. Imai, *ECS Trans.*, 2012, **50**, 1759–1767.
37. J. Bonde, P. G. Moses, T. F. Jaramillo, J. K. Nørskov, I. Chorkendorff, *Faraday Discuss.*, 2009, **140**, 219–231.
38. S. Sata, M. I. Awad, M. S. El-Deab, T. Okajima, T. Ohsaka, *Electrochim. Acta*, 2010, **55**, 3528–3536.
39. H. J. Mathieu, D. Landolt, *Surf. Interface Anal*, 1983, **5**, 77–82.
40. B. Díaz, J. Światowska, V. Maurice, A. Seyeux, E. Härkönen, M. Ritala, S. Tervakangas, J. Kolehmainen, P. Marcus, *Electrochim. Acta*, 2013, **90**, 232–245.
41. K. Müller, G. Lefevre, *Langmuir*, 2011, **27**, 6830–6835.
42. D. A. Sverjensky, K. Fukushi, *Environ. Sci. Technol.*, 2006, **40**, 263-271.
43. J. A. Davis, L.O. Leckie, *J. Colloid Interface Sci.*, 1980, **74**, 32−43.
44. X. Xie, W. Mu, X. Li, H. Wei, Y. Jian, Q. Yu, R. Zhang, K. Lu, H. Tang, S. Luo, *Electrochim. Acta*, 2014, **134**, 201–208.
45. B. Børresen, G. Hagen, R. Tunold, *Electrochim. Acta*, 2002, **47**, 1819–1827.
46. A Phuruangrat, D. J. Ham, S. J. Hong, S. Thongtem, J. S. Lee, *J. Mater. Chem.*, 2010, **20**, 1683–1690.
47. H. Zheng, M. Mathe, *Int. J. Hydrogen Energy*, 2011, **36**, 1960–1964.
48. N. Spataru, J. G. Le Helloco, R. Durand, *J. Appl. Electrochem.*, 1996, **26**, 397–402.
49. X. Z. Yuan, H. Li, S. Zhang, J. Martin, H. Wang, *J. Power Sources*, 2011, **196**, 9107–9116.
50. W. F. Chen, J. T. Muckerman, E. Fujita, *Chem. Comm.*, 2013, **49**, 8896-8909.
51. A. Kishimoto, T. Kudo, T. Nanba, *Solid State Ionics*, 1992, **53**, 993–997
52. A. B. Yaroslavtsev, A. E. Nikolaev, *Mendeleev Comm.*, 1995, **5**, 136–137.

53. V. Macagno, J. W. Schultze, *J. Electroanal. Chem.*, 1984, **180**, 157–170.

54. T. Saito, Y. Ushio, M. Yamada, T. Niwa, *Solid State Ionics*, 1990, **40**, 499–501.

55. J. Kibsgaard, Z. Chen, B. N. Reinecke, T. F. Jaramillo, *Nat. Mater.*, 2012, **11**, 963–969.

56. Y. Hou, B. Zhang, Z. Wen, S. Cui, X. Guo, Z. He, J. Chen, *J. Mater. Chem. A*, 2014, **2**, 13795-13800.

57. N. Singh, J. Hiller, H. Metiu, E. McFarland, *Electrochim. Acta*, 2014, **145**, 224–230.

Table 1. Binding energies of Ta $4f_{5/2}$ obtained at TaO_x/GC electrode before and after the electrochemical treatment for 30 and 1000 cycles. The Ar^+ etching was performed for 1 min.

Condition of TaO_x/GC electrodes	Binding energy (±0.1eV)							
	Ta^{5+}		Ta^{4+}		Ta^{3+}		Ta^{2+}	
	Before	After Ar^+ etching	Before	After Ar^+ etching	Before	After Ar^+ etching	Before	After Ar^+ etching
As-prepared	28.7	28.9	–	27.9	–	26.2	–	25.2
After 30 cycles	29.0	28.6	28.3	28.0	–	–	–	–
After 1000 cycles	29.1	28.8	28.4	27.9	–	26.1	–	–

Figures caption

Figure 1. Optical surface images obtained at (**a**) the TaO_x/GC electrodes before and after the electrochemical reduction treatment for 1000 cycles, (**b**) bare GC plate, (**c**) TaO_x on the GC plate, and (**d**) the treated TaO_x on GC plate for 30 cycles.

Figure 2. SEM images of the TaO_x/GC (**a** and **c**) as-prepared and (**b** and **d**) after the electrochemical reduction treatment for 30 cycles.

Figure 3. TEM images of the TaO_x/GC (**a, c and e**) as-prepared and (**b, d and f**) after the electrochemical reduction treatment for 30 cycles. (**g**) EDX spectrum obtained for the region of (**f**) showing some sulfur (S)-containing species. The red arrows point out black-dotted regions which might be associated with the presence of S-containing species.

Figure 4. XPS spectra of (**a**) survey scan, (**b**) high resolution of S 2p, (**c**) O 1s and (**d**) C 1s obtained at the TaO_x/GC as-repared and after the electrochemical reduction treatment for 30 and 1000 cycles.

Figure 5. Ta 4f XPS spectra obtained at the TaO_x/GC as-prepared and after the electrochemical reduction treatment for 30 and 1000 cycles (**a**) before and (**b**) after Ar^+ etching for 1 min.

Figure 6. (**a**) A plot of potential at current of −1 mA cm^{-2} versus number of potential cycling obtained at the TaO_x/GC electrode during the electrochemical reduction treatment in 2 M H_2SO_4 solution at scan rate of 20 mV s^{-1}. (**b**) Linear sweep voltammograms (LSVs) obtained at the TaO_x/GC in 0.5 M H_2SO_4 solution at scan rate of 5 mV s^{-1} in which all electrodes were previously treated by the electrochemical reduction treatment for up to 1000 cycles.

Figure 7. LSVs obtained at the TaO_x/GC and bare GC electrodes in O_2-saturated 0.1 M H_2SO_4 solution at scan rate 10 mV s^{-1} in which the two electrodes were

previously treated by the electrochemical reduction treatment for 1000 cycles. The inset figure shows the magnified curves to determine the onset potential.

Figure 8. A plot of current at potential of −200 mV versus number of potential cycling during the durability test obtained at the reduced TaO_x/GC electrode which was previously treated by the electrochemical reduction treatment for 1000 cycles. The test was performed by potential scanning between −0.2 and 1.23 V in N_2-saturated 0.5 M H_2SO_4 solution. The inset figure shows the magnified graph at the first 100 cycles showing a dramatic enhancement of HER for the first 10 cycles.

Figures

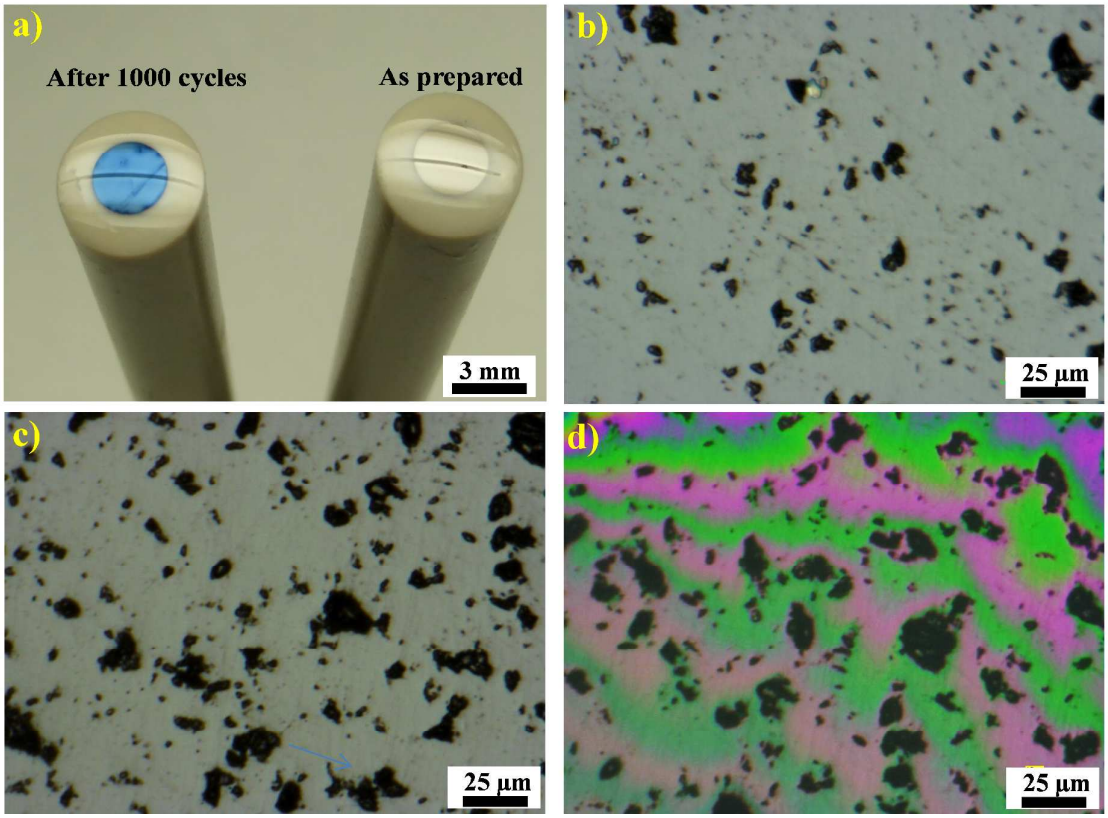

Figure 1. Awaludin et al.

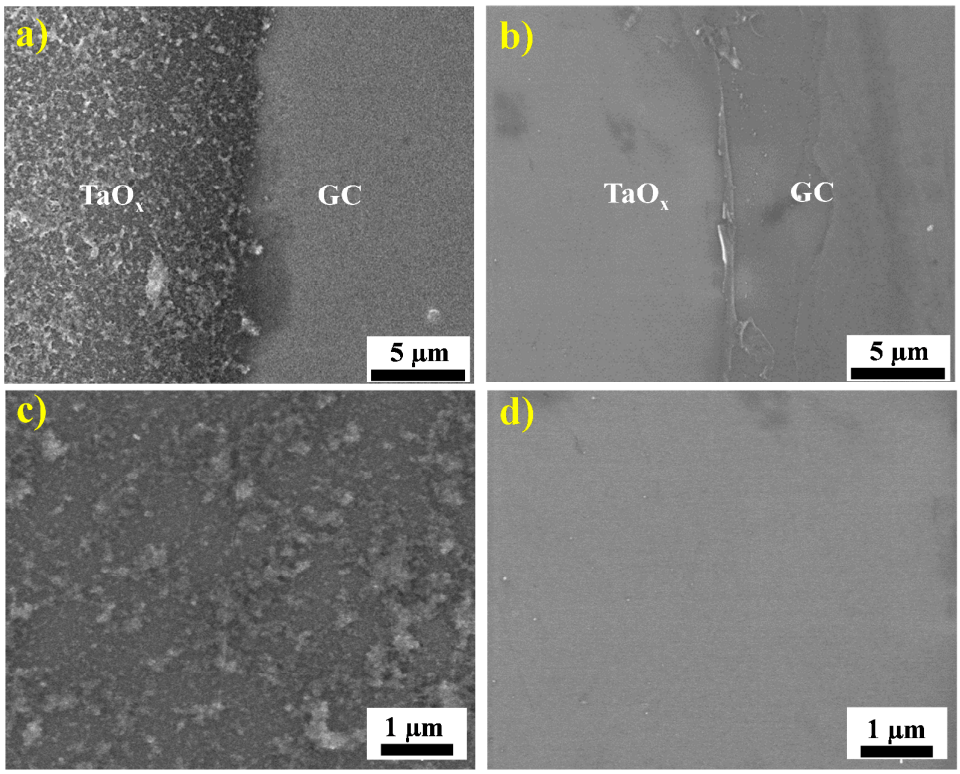

Figure 2. Awaludin et al.

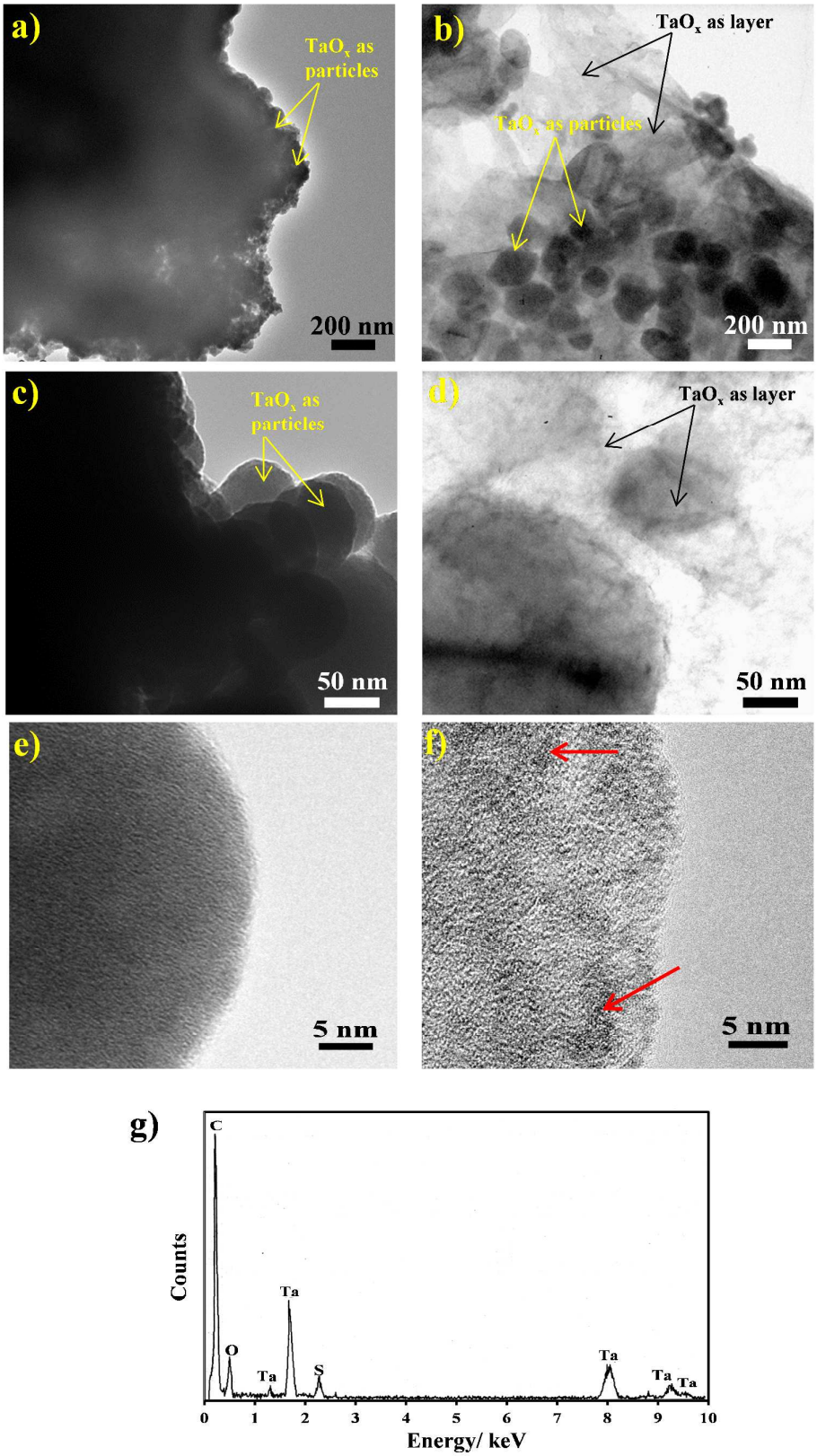

Figure 3. Awaludin et al.

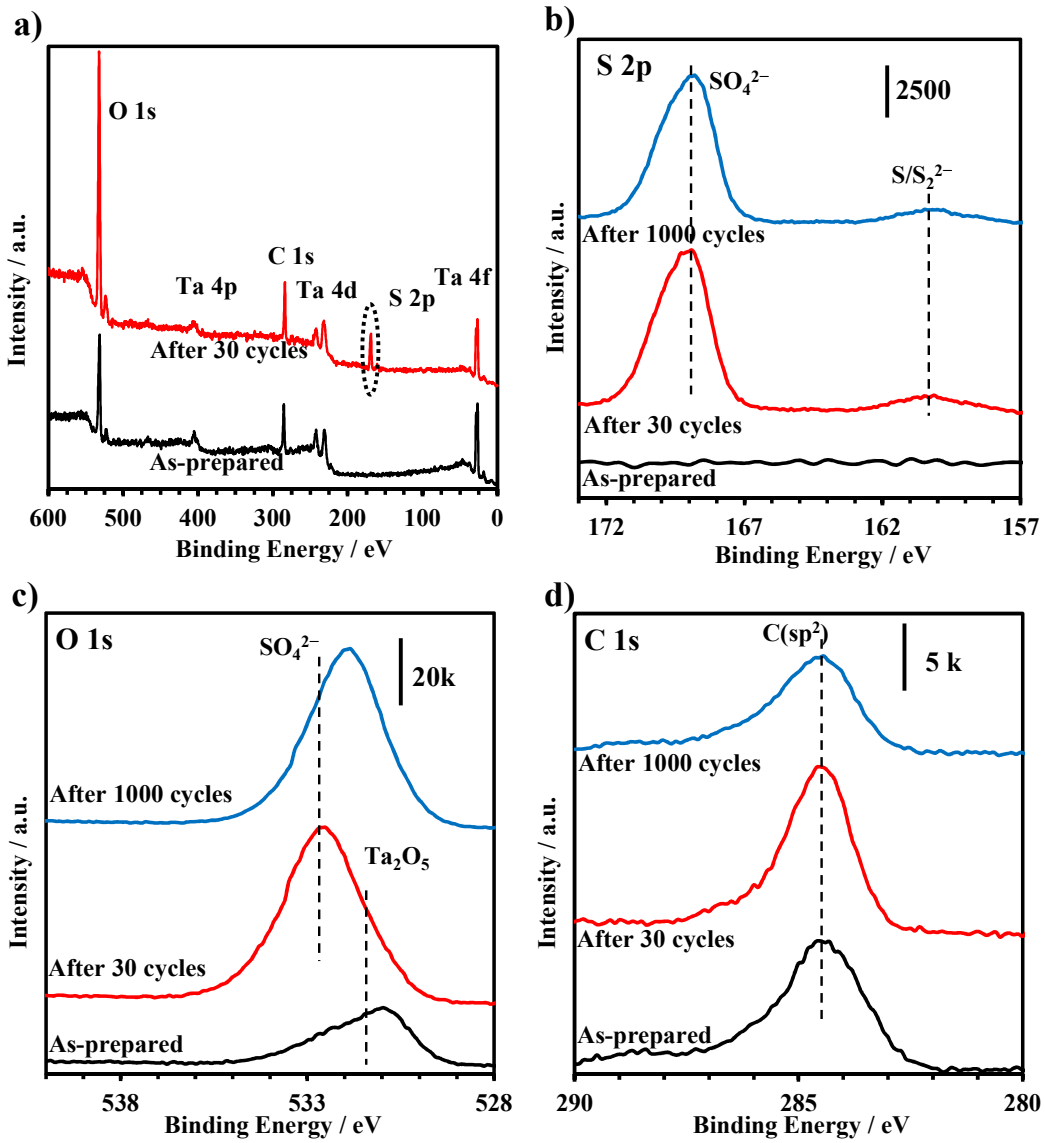

Figure 4. Awaludin et al.

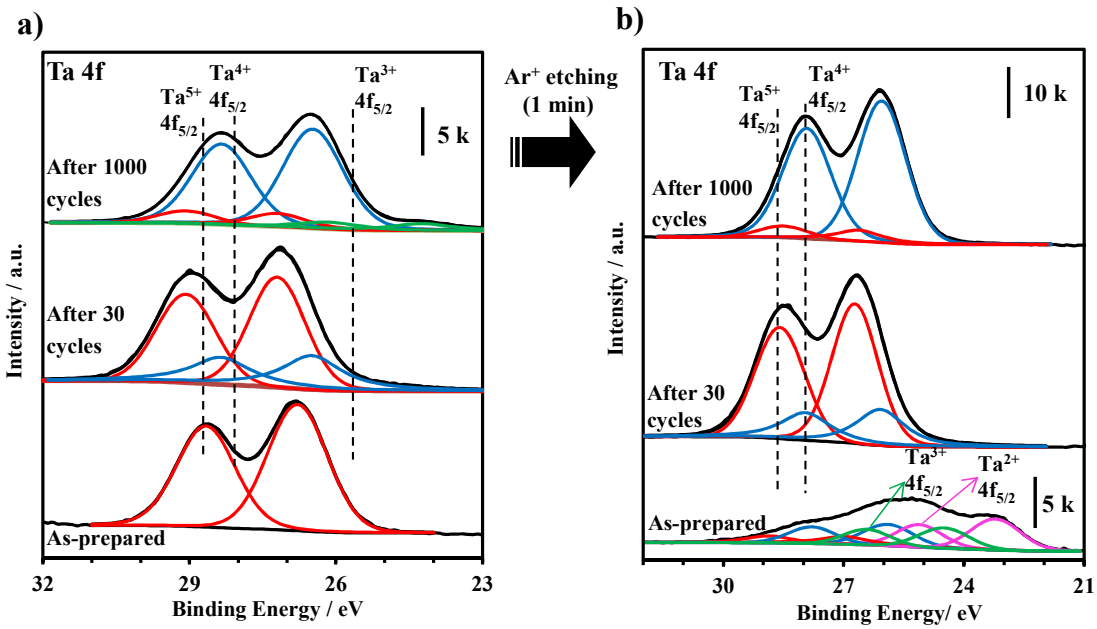

Figure 5. Awaludin et al.

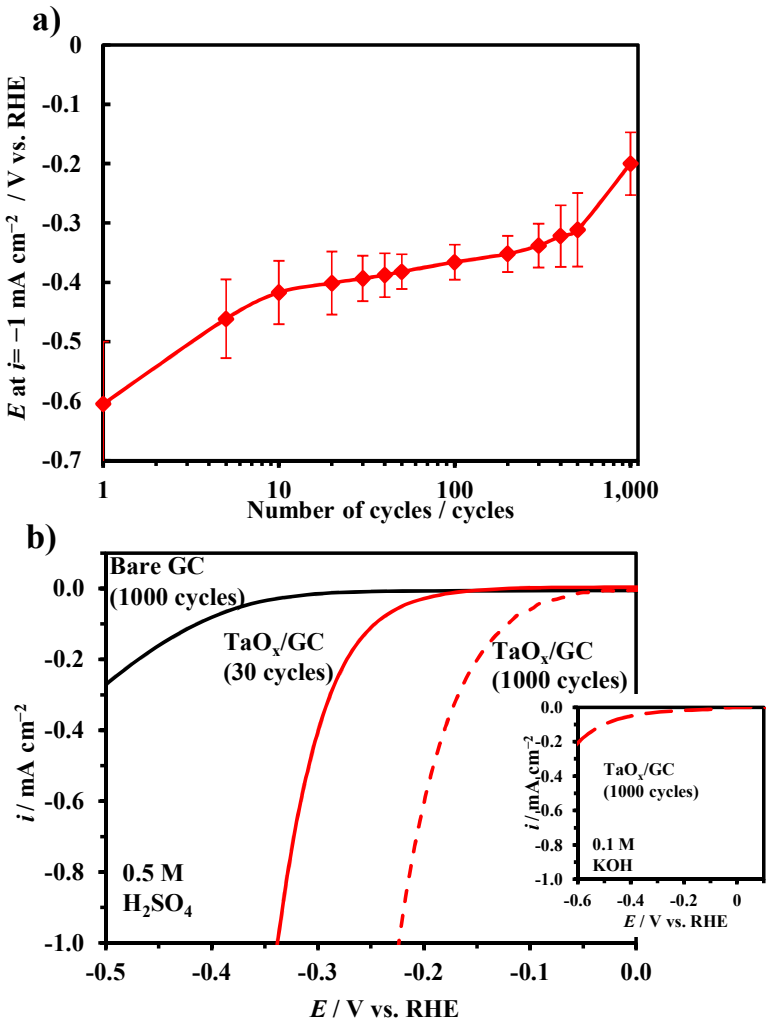

Figure 6. Awaludin et al.

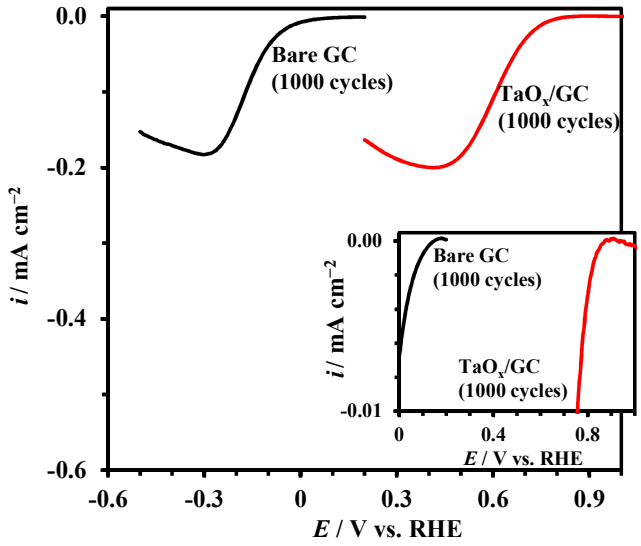

Figure 7. Awaludin et al.

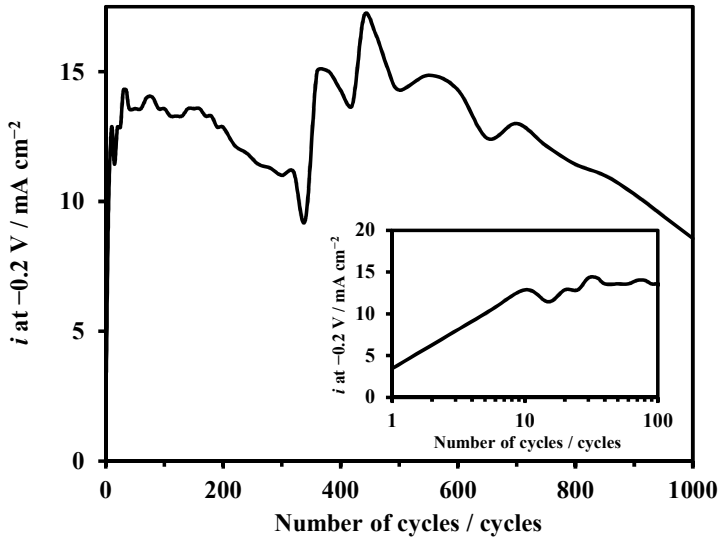

Figure 8. Awaludin et al.

Graphical abstract